Inorganic Chemistry
Cite This: Inorg. Chem. 2018, 57, 9748−9756
Forum Article
pubs.acs.org/IC

Immobilization of an Amphiphilic Molecular Cobalt Catalyst on Carbon Black for Ligand-Assisted Water Oxidation

Habib Baydoun,[†] Jordyn Burdick,[†] Bishnu Thapa,[†] Lanka Wickramasinghe,[†] Da Li,[†] Jens Niklas,[‡] Oleg G. Poluektov,[‡] H. Bernhard Schlegel,[†] and Cláudio N. Verani*[,†]

[†]Department of Chemistry, Wayne State University, 5101 Cass Avenue, Detroit, Michigan 48202, United States
[‡]Chemical Sciences & Engineering Division, Argonne National Laboratory (ANL), Lemont, Illinois 60439, United States

Supporting Information

ABSTRACT: We have prepared the amphiphilic molecular catalyst $[Co^{III}(L^{OC_{18}})(pyrr)_2]ClO_4$ (**1**), where $L^{OC_{18}}$ is the deprotonated form of *N*,*N*′-[4,5-bis(octadecyloxy)-1,2-phenylene]dipicolinamide. Species **1** can be anchored onto a carbon black support to yield the assembly **1@CB**, which can catalyze water oxidation at an affordable onset overpotential of 0.32 V, with a current density of 10 mA/cm^2 at 0.37 V. Moreover, **1@CB** displays TOF = 3850 h^{-1}. A mechanism is proposed based on the experimental and density-functional-theory-calculated data.

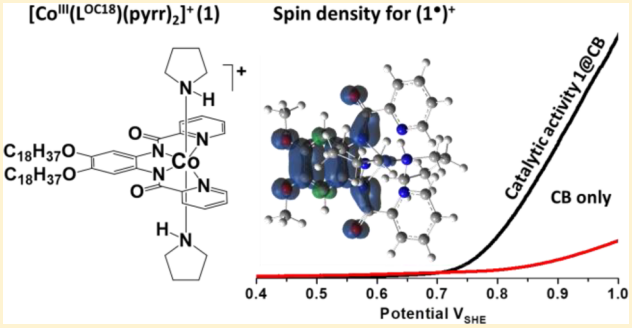

INTRODUCTION

Surface functionalization is pivotal to enable the use of homogeneous catalysts anchored onto conductive solid supports. In this manner, future integrated water-splitting devices can be developed in which water oxidation occurs at the anode and proton reduction occurs at the cathode. Traditionally, such electrodes are made with solid-state materials such as metal oxides or phosphides. However, understanding the surface chemistry of such extended and tridimensional materials is challenging. On the other hand, understanding and modifying the chemistry of surfaces via functionalization with discrete and molecular coordination complexes is more attainable because of the well-known and tunable electronic signatures of molecular materials. As such, improving the catalytic activity can be achieved using rational ligand design along with electrochemical and spectroscopic methods.

The water-splitting reaction involves two half-reactions: water oxidation and proton reduction. With a standard potential of 1.23 V_{SHE}, water oxidation is the more energetically demanding of the two half-reactions. This high-energy requirement is imparted by the need to perform four-electron chemistry and form O−O bonds. The mechanisms of water oxidation require the formation of high-valent oxo (M^{IV}=O or M^{V}=O) or hydroperoxo (M^{III}OOH) species. In order to lower the activation barrier required to reach such highly oxidized states needed for catalysis, redox-active ligands have been utilized.[1,2] This is due to the formation of a radical-based species instead of the expected high-valent tautomer[3] in the electron-transfer sequence $[M^{n-1}L]^0 \xrightarrow{-e^-} [M^{n-1}L^{\bullet}]^+ \rightleftharpoons [M^{n}L]^+$. When the last equilibrium step favors the $[M^{n-1}L^{\bullet}]^+$ product, the oxidized ligand acts as a relevant electron reservoir but is prone to degradation.

Recent efforts have focused on anchoring molecules onto conductive solid supports in an attempt to favor the high-valent $[M^{n}L]^{n+}$ product, enhancing the robustness of catalysts and favoring water splitting.[4−6] We have recently shown that physisorbed Langmuir−Blodgett films of a procatalytic phenolate-rich cobalt complex are effective on fluorine-doped tin oxide.[7] The resulting modified electrode is an excellent water oxidation catalyst with an overpotential of 0.5 V. However, structural rearrangement takes place after a potential bias is applied. This transformation, coupled with the labor-intensive layer-by-layer deposition process, precludes the large-scale application of the approach.

Produced by the incomplete combustion of petrochemicals, carbon black (CB) has been used as a solid support along with Nafion to drive catalytic water oxidation.[8−10] As such, we hypothesized that CB can be functionalized with an amphiphilic metal complex and that van der Waals interactions between the substrate and complex will lead to more robust water oxidation catalysts. Therefore, similar to other systems that we reported in the recent past,[7,11−13] we designed a new ligand with two octadecyloxy groups incorporated into the backbone. These alkoxy groups play important functions: (i) they serve as hydrophobic backbones to anchor the molecule onto CB, and

Special Issue: Applications of Metal Complexes with Ligand-Centered Radicals

Received: January 2, 2018
Published: May 14, 2018

DOI: 10.1021/acs.inorgchem.7b03252
Inorg. Chem. 2018, 57, 9748−9756

Scheme 1. Synthesis of 1, with R = $C_{18}H_{37}$

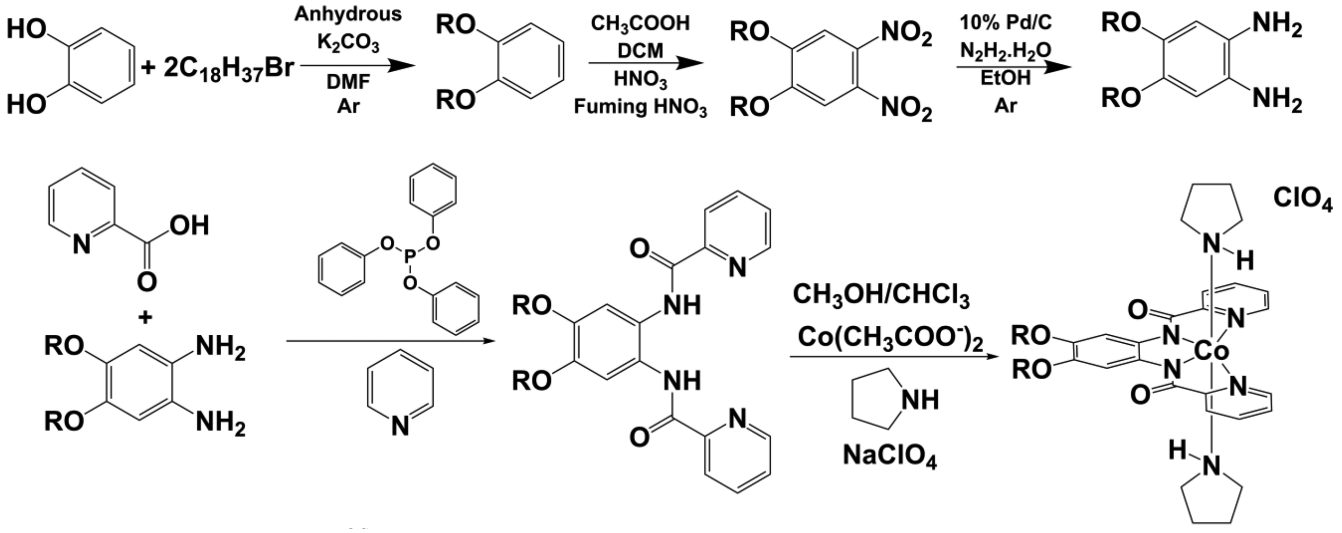

(ii) they lower the oxidation potential required for water oxidation.

RESULTS AND DISCUSSION

The ligand $H_2L^{OC_{18}}$ was prepared via the multistep synthetic route outlined in Scheme 1, which involved the functionalization of catechol with octadecyl groups to produce bis(octadecyloxybenzene).[7,12,14,15] This precursor was then nitrated, yielding 1,2-dinitro-4,5-bis(octadecyloxy)benzene, which was subsequently reduced to form the air-sensitive precursor 4,5-bis(octadecyloxy)benzene-1,2-diamine. The diamine was treated with picolinic acid to yield the ligand *N*,*N*′-[4,5-bis(octadecyloxy)-1,2-phenylene]dipicolineamide, $H_2L^{OC_{18}}$.[16]

The complex $[Co^{III}(L^{OC_{18}})(pyrr)_2]ClO_4$ (**1**) contains a doubly deprotonated $(L^{OC_{18}})^{2-}$ ligand and was prepared following a modification to the previously reported procedure[17,18] in which stoichiometric amounts of $H_2L^{OC_{18}}$ were treated with cobalt acetate in the presence of pyrrolidine. After stirring under aerobic conditions, **1** was precipitated using $NaClO_4$. Catalyst **1** was thoroughly characterized using ^1H NMR, Fourier transform infrared (FTIR), mass spectrometry, and elemental analysis. A strong peak in the FTIR spectrum at 1091 cm^{-1} confirmed the presence of a perchlorate counterion. This observation, coupled with the occurrence of sharp peaks in the NMR spectrum (Figure S1), suggests that we have formed a cobalt(III) complex in a pseudooctahedral $^{LS}3d^6$ environment. High-resolution mass spectrometry shows a peak cluster at m/z 911.5825 corresponding to the metal complex without the two axial pyrrolidines. The elemental analysis results confirm these structural assignments.

The cyclic voltammogram of **1** was taken in dichloromethane (CH_2Cl_2) in the presence of tetrabutylammonium hexafluorophosphate ($TBAPF_6$) as the supporting electrolyte using ferrocene as an internal standard.[19] The cyclic voltammogram (Figure 1) shows four independent redox events consisting of two oxidative and two reductive processes. The irreversible reductive processes at −0.36 and −1.12 V_{SHE} (E_{pc}) are tentatively assigned as the sequential reduction from Co^{III} $3d^6$ to Co^{II} $3d^7$ and then Co^{II} to Co^{I} $3d^8$. Two oxidation processes at 0.91 V_{SHE} (ΔE = 92 mV; $|I_{pa}/I_{pc}|$ = 0.94) and 1.41 V_{SHE} (ΔE = 94 mV; $|I_{pa}/I_{pc}|$ = 1.45) are respectively associated with the

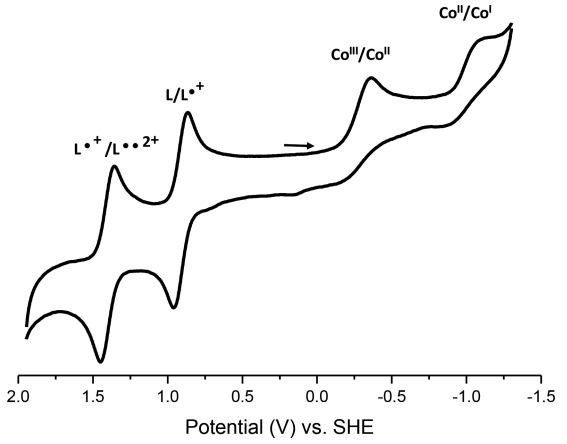

Figure 1. (a) Cyclic voltammogram of **1** (1 mM) in CH_2Cl_2, with $TBAPF_6$ as the supporting electrolyte, glassy carbon as the working electrode, Ag/AgCl as the reference electrode, and platinum wire as the auxiliary electrode.

generation of the formal high-valent Co^{IV} $3d^5$ and possibly Co^{V} $3d^4$ species but have been rather described as amido to amidyl radical transformations in unsubstituted systems.[20,21] It is interesting to note that compared to our previously studied and structurally related $[Co^{III}(L)(pyrr)_2]PF_6$ (**2**) system with a similar nonalkoxy-functionalized ligand, the current oxidation processes occur at potentials that are about 0.5 V less positive.[22] This decrease in the oxidative potential is associated with the electron-donating effect of the alkoxy chains.[6]

The X-band electron paramagnetic resonance (EPR) spectrum of the electrochemically generated singly oxidized cobalt complex, nominally $[Co^{IV}(L^{OC_{18}})(pyrr)_2]^{2+}$, revealed a narrow isotropic signal at g = 2.00, close to the free-electron g value, with a line width of 3.5 mT (Figure 2). The typical EPR signals expected for either high-spin or low-spin (LS) cobalt(IV) complexes are absent.[23−25] Therefore, the observed spectrum is consistent with an $S = {}^1/_2$ state associated with the formation of a radical-bearing species like $[Co^{III}(L^{OC_{18}}\bullet)(pyrr)_2]^{2+}$. These conclusions are also supported by density functional theory (DFT) calculations. For this $S = {}^1/_2$ state, the spin-density plot (Figure 3a) revealed a delocalized unpaired electron on the diamine moiety of the ligand rather than on the

DOI: 10.1021/acs.inorgchem.7b03252
Inorg. Chem. 2018, 57, 9748−9756

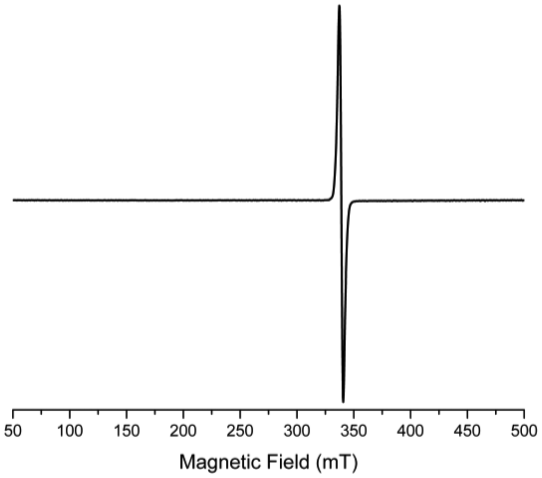

Figure 2. cw X-band EPR spectrum of the electrochemically singly oxidized cobalt complex (nominally $[Co^{IV}(L^{OC_{18}})(pyrr)_2]^{2+}$) in CH_2Cl_2 at T = 30 K.

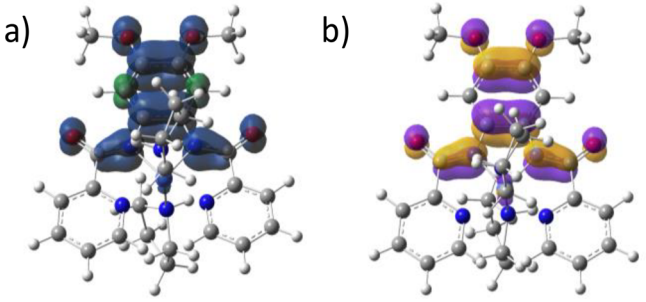

Figure 3. (a) Spin-density plot for $[Co^{III}(L^{OC_{18}\bullet})(pyrr)_2]^{2+}$ and (b) the LUMO for $[Co^{III}(L^{OC_{18}\bullet\bullet})(pyrr)_2]^{3+}$.

metal center. This observation is in line with our previous report on the redox activity of phenylenediamine bridging moieties.[26]

The doubly oxidized species is most stable as a diamagnetic singlet (S = 0) with no observable spin density because of its closed shell. However, the lowest unoccupied molecular orbital (LUMO; Figure 3b) was calculated as ligand-based. These data suggest the assignment of the second oxidation as being ligand-based like the first oxidation and best described as $[Co^{III}(L^{OC_{18}\bullet\bullet})(pyrr)_2]^{3+}$.

Although our observations agree with previous assignments[20,21] that favor the formation of ligand radicals, Åkermark et al.[27] have shown that a related ruthenium complex can efficiently catalyze water oxidation. Furthermore, Kim and co-workers[28−30] have shown that iron, cobalt, and manganese ions act as oxygen-atom-transfer agents in similar $[N_4]$ planar environments and that high-valent oxo species were observed in situ. These same oxo species stabilized during oxygen-atom transfer are essential intermediates in the water oxidation mechanism. These observations suggest that the species $[Co^{III}(L^{OC_{18}\bullet})]^+$ and the putative $[Co^{IV}(L^{OC_{18}})]^+$ may be very close in energy because the latter cannot be calculated without converging into the former. As such, an oxo species may be better described as nominally $[Co^{IV}{=}O(L^{OC_{18}})]^+$. Therefore, we hypothesized that **1** could perform water oxidation as a molecular catalyst. The evaluation of these results allows us to infer whether the metal or the bis(amidopyridine) ligand is associated with the high oxidation state required for catalysis. In order to assess the catalytic properties of **1**, we anchored the molecule onto the surface of CB to yield an assembly denoted as **1@CB**. This was done by adding a solution of **1** to a suspension of CB in CH_2Cl_2. Then, ethanol was added to precipitate the resulting suspension. The precipitate was isolated by centrifuging the sample. Following decantation of the supernatant, the precipitate was dried overnight under ambient conditions and resuspended using a 2:1:1:1 mixture of ethanol/isopropyl alcohol/water/Nafion. The sample was ultrasonicated to form the homogeneous ink that was used in the catalysis. Inductively coupled plasma mass spectrometry (ICP-MS) analysis of the final ink revealed that 70% of the cobalt present in the initial solution was anchored on CB. The FTIR spectra of **1**, **CB**, and **1@CB** (Figure S2) show that the characteristic peaks of **1** (where CB does not have significant absorption) are retained in the ink, thus indicating that molecular deposition took place without major structural changes. Unfortunately, attempts to prepare a similar ink based on the unsubstituted $[Co^{III}(L)(pyrr)_2]ClO_4$ (**2**)[22] were unsuccessful.

The **1@CB** ink was tested for catalysis using a rotating-disk electrode operating at 1600 rpm in a 1 M potassium hydroxide (KOH) solution. Figure 4a shows the *iR*-corrected polarization curves obtained for **1@CB** (black trace) in comparison to the blank CB (red trace). Significant current enhancement is attained by **1@CB** with an onset overpotential of 0.32 V. At an overpotential of 0.37 V, the current density reaches 10 mA/cm^2, an important figure of merit in the development of solar cells operating at 10% efficiency.[31] Remarkably, **1@CB** has an

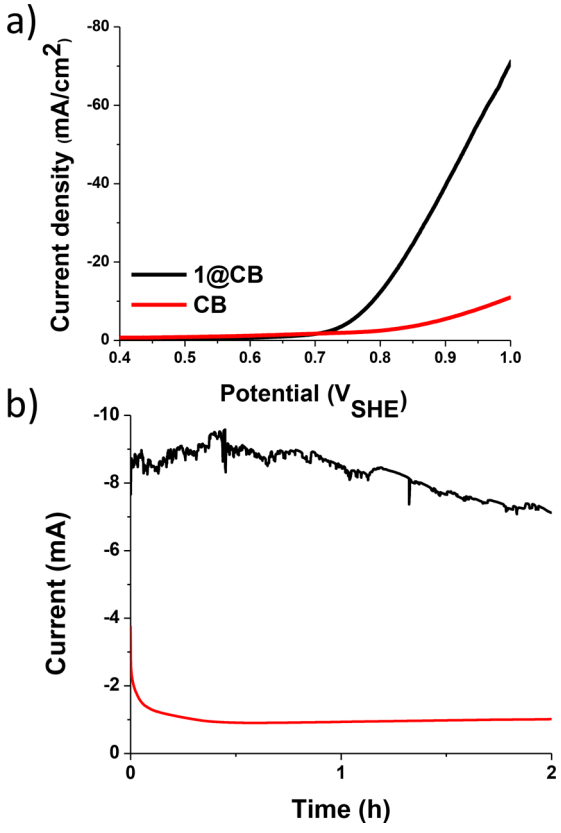

Figure 4. (a) Polarization curves for **1@CB** and the blank CB in a 1 mol/L KOH solution of pH 14 [RDE glassy carbon 1600 rpm (WE), Ag/AgCl (RE), Pt wire (AE)]. (b) Plot of current versus time, under an applied potential of 0.7 $V_{Ag/AgCl}$ (0.89 V_{SHE}) for a 2 h catalytic run.

DOI: 10.1021/acs.inorgchem.7b03252
Inorg. Chem. 2018, 57, 9748−9756

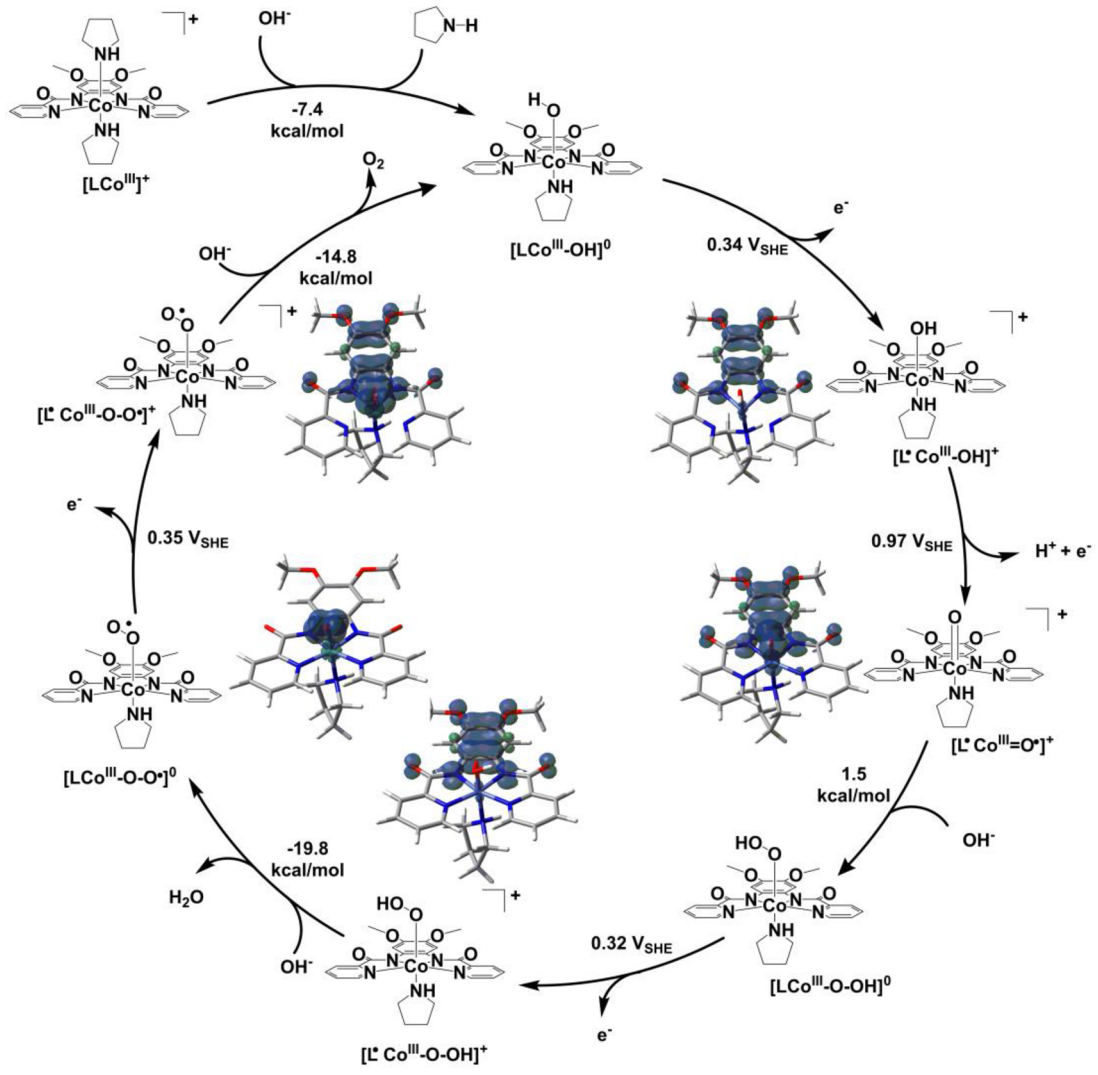

Figure 5. Proposed water oxidation mechanism of $[Co^{III}(L^{OCH_3})(pyrr)_2]^+$. Spin-density plots are shown next to the paramagnetic species (isovalue = 0.04 au).

overpotential at 10 mA/cm^2 on par with recently reported nanostructured materials.[8,9,31−34]

To evaluate the catalytic activity of **1@CB**, we performed a bulk electrolysis experiment to determine the turnover number (TON) using a custom-built H-type electrocatalytic cell. The ink was deposited onto a carbon cloth working electrode, which was then used during catalysis. Following 2 h of electrolysis at an applied potential of 0.89 V_{SHE} (overpotential = 0.49 V), 154 μmol of oxygen were produced that matched very well with the theoretical amount of oxygen based on the net charge consumption of 155 μmol (50.9 C). Considering that the initial amount of cobalt present on the surface is estimated as 0.02 μmol, the assembly underwent 7700 turnovers, well above other molecular catalysts in solution.[35−38] This TON value corresponds to an observed averaged turnover frequency of 3850 h^{-1} and a near-quantitative Faradaic efficiency of 99%. Figure 4b shows the plot of current versus time. The slight decrease in the current observed during catalysis suggests that the catalyst is undergoing a slow deactivation process in which the cobalt is possibly leaching out of the electrode. On the basis of the recently published behavior of the analogous unsubstituted **2** toward water reduction,[22] this deactivation is likely due to the formation of a ligand-based radical during the catalytic cycle.[39] Indeed, ICP-MS analysis of the postcatalytic solution reveals the presence of 4 ppb of cobalt ion, against trace amounts below the detection limit for the blank.

We also performed X-ray photoelectron spectroscopy (XPS) analysis on **1@CB** to assess whether the surface-immobilized molecules of **1** rearrange into CoO_x-based nanoparticulates. The results shown in Figure S3 reveal that the Co $2p_{3/2}$ and Co $2p_{1/2}$ energy peaks, respectively at 781 and 796 eV, remain unchanged before and after catalysis. This observation was further confirmed using electrochemical measurements (Figure S4). We observed an electrochemical process at 0.08 V_{SHE} before catalysis, which we ascribed to the Co^{III}/Co^{II} couple. As expected for molecular catalysts, the process remained intact after catalysis. These results point out that the molecular nature of species **1** persists during catalysis.

In general, O−O bond formation can occur via two possible pathways in the water oxidation mechanism. In the first pathway, two Co=O species combine to form a μ-peroxo bridging intermediate (Co−O−O−Co). This mechanism is unlikely to be present here because **1** is anchored onto CB with limited surface mobility. We therefore favor a second pathway in which a nucleophilic attack by OH^- onto the Co=O species takes place. This possibility was evaluated using DFT

DOI: 10.1021/acs.inorgchem.7b03252
Inorg. Chem. 2018, 57, 9748−9756

calculations on a truncated analogue where $-OCH_3$ replaces $-OC_{18}H_{37}$, and our results suggest that catalysis is initiated by the substitution of one pyrrolidine by a hydroxide ion, yielding $[Co^{III}(L^{OCH_3})(pyr)(OH)]^0$ (Figure 5). This transformation is favored by 7.4 kcal/mol. The catalytic cycle ensues with $[Co^{III}(L^{OCH_3})(pyr)(OH)]^0$ undergoing a one-electron oxidation to yield the ligand-oxidized $[Co^{III}(L^{OCH_3}\bullet)(pyr)(OH)]^+$ at a potential of 0.34 V_{SHE}. Following this step, a proton-coupled electron transfer takes place to form the formally $[Co^{IV}{=}O]$-containing species $[Co^{III}(L^{OCH_3}\bullet)(pyr)(oxo^\bullet)]^+$ at 0.97 V_{SHE}. It is important to note that the unpaired electron on $[Co^{III}{=}O^\bullet]$ is significantly delocalized over the metal center (Mulliken spin densities of 0.11 on cobalt and 0.89 on oxo; Table S3). Although the calculated potential for this step appears to be higher than the experimentally determined onset potential, this difference is well within the accepted values associated with DFT-calculated electrochemical potentials.[40] Then an isothermal transformation (ΔG = 1.5 kcal/mol) in which a nucleophilic attack by OH^- onto the Co=O oxyl species takes place forms the diamagnetic hydroperoxo $[Co^{III}(L^{OCH_3})(pyr)(OOH)]^0$. Species $[Co^{III}(L^{OCH_3})(pyr)(OOH)]^0$ undergoes a one-electron oxidation at 0.32 V_{SHE} to yield $[Co^{III}(L^{OCH_3}\bullet)(pyr)(OOH)]^0$, which is deprotonated into a superoxide species described as $[Co^{III}(L^{OCH_3})(pyr)(OO\bullet)]^+$ (ΔG = −19.8 kcal/mol). Following a further one-electron oxidation to form $[Co^{III}(L^{OCH_3}\bullet)(pyr)(OO^\bullet)]^+$ at 0.35 V_{SHE}, a nucleophilic attack by OH^- takes place to release O_2 and regenerate $[Co^{III}(L^{OCH_3})(pyr)(OH)]^0$. It is interesting to note that throughout our transformations the oxidation state of the metal remains largely unchanged at $[Co^{III}]$, while the ligand acts as the site were oxidizing equivalents are stored. This is in contrast to most other reported systems in which pure metal oxidation or highly limited ligand involvement are assumed.[2,41−46]

CONCLUSION

In conclusion, we have reported on a novel alkoxy-substituted cobalt complex that can be anchored onto CB. The resulting **1@CB** assembly, suspended in ink form, catalytically oxidizes water under basic conditions with an affordable onset overpotential of 0.32 V. The assembly reaches the required current density of 10 mA/cm^2 needed for solar cell development at an overpotential of just 0.37 V, while retaining its molecular nature. The affordable potentials are associated with ligand oxidation, thus acting as an electron reservoir that effectively lowers the activation barrier needed for catalysis. This involvement, however, leads to slow catalyst deactivation by demetalation due to an unfavorable equilibrium involving $[M^{n-1}L\bullet]^+ \leftrightharpoons [M^nL]^+$. As such, while observed TONs reached notable values above 5000 for molecular catalysts, improvements in design will be necessary to allow for the formation of high-valence cobalt species expected to enhance the stability of the catalyst.

EXPERIMENTAL SECTION

Materials and Characterization. Ultrapure water (18.1 MΩ.cm) was used in all manipulations. All other solvents and reagents were from commercial sources and were not further purified. ^{1}H NMR spectra were recorded on a Varian 400 or 600 MHz spectrometer. FTIR spectra were recorded on a Bruker Tensor 27 spectrometer using potassium bromide (KBr) pellets recorded between 4000 and 600 cm^{-1}. Elemental analysis was performed by Midwest Microlabs, Indianapolis, IN, and measured using an Exeter CE440 CHN analyzer. Cyclic voltammograms in organic solvents were recorded using a BAS 50W electrochemical analyzer. $TBAPF_6$ was used as the supporting electrolyte, Ag/AgCl was used as the reference electrode (RE), and a platinum wire was used as the auxiliary electrode (AE). The cyclic voltammograms were recorded under an argon atmosphere, and ferrocene was added as an internal standard at a scan rate of 0.1 V/s.[19] XPS spectra were recorded using a Kratos Axis Ultra X-ray photoelectron spectrometer, and all of the spectra were calibrated using C 1s at 284.8 eV as a charge reference. XPS spectra of the electrode itself did not show any discernible cobalt peaks; therefore, functionalized CB was removed from the surface of the electrode by sonicating it in ethanol. Then ethanol was removed, and the concentrated sample was used for XPS analysis.

Synthesis of 1,2-Bis(octadecyloxy)benzene. A solution of 1-bromooctadecane (23.4 g, 70.2 mmol) in dimethylformamide (DMF; 70 mL) was added dropwise under inert conditions to a solution of catechol (3.50 g, 31.8 mmol) and anhydrous potassium carbonate (16.0 g, 116 mmol) in anhydrous DMF (53 mL). The reaction was allowed to reflux for 18 h, after which it was poured into ice-cold water (150 mL) and subsequently extracted with CH_2Cl_2 (100 mL). The organic layer was dried over anhydrous sodium sulfate (Na_2SO_4). The solvent was removed by rotary evaporation, and the remaining yellow oil was dissolved in a 19:1 mixture of hexane and ethyl acetate. The solution was filtered through silica under vacuum. The isolated yellow solution was concentrated to half of its original volume and refrigerated to yield a white precipitate. Yield: 72%. ESI: m/z^+ 637.5892 (100%) for $[C_{42}H_{78}O_2 + Na^+]$. IR (KBr, cm^{-1}): 2850−2919 (ν_{C-H}), 1595 ($\nu_{C=C}$), 1508 ($\nu_{C=C}$), 1259 (ν_{C-O-C}). ^{1}H NMR ($CDCl_3$, 400 MHz): δ 6.866 (s, 4H^{Ph}), 3.969 (t, 4H^{OCH_2}), 1.792 (m, 4H^{CH_2}), 1.444 (m, 4H^{CH_2}), 1.239 (s, 56H^{CH_2}), 0.863 (t, 6H^{CH_3}).

Synthesis of 1,2-Dinitro-4,5-bis(octadecyloxy)benzene. The compound 1,2-bis(octadecyloxy)benzene (2.05 g; 3.33 mmol) was dissolved in 48 mL of a 1:1 CH_2Cl_2/acetic acid mixture. The reaction mixture was subsequently placed in an ice bath, and 3.50 mL of nitric acid was added. Following the addition, the reaction was stirred at room temperature for 30 min and then cooled back in an ice bath, when 8.50 mL of fuming HNO_3 was added. Then the reaction mixture was stirred at room temperature for 72 h before being poured into ice-cold water (100 mL, 0 °C). The organic layer was washed with (3 × 100 mL) saturated $NaHCO_3$ and a brine solution. The organic layer was subsequently dried over Na_2SO_4. The organic solvent was removed by rotary evaporation and recrystallized from acetone to yield yellow crystals. Yield: 86%. ESI: m/z^+ 743.5341 (100%) for $[C_{42}H_{76}N_2O_6 + K^+]$. IR (KBr, cm^{-1}): 2850−2918 (ν_{C-H}), 1587 ($\nu_{C=C}$), 1539 ($\nu_{C=C}$), 1466 ($\nu_{N=O}$), 1335 ($\nu_{N=O}$), 1294 (ν_{C-O-C}). ^{1}H NMR ($CDCl_3$, 400 MHz): δ 7.270 (s, 2H^{Ph}), 4.073 (t, 4H^{OCH_2}), 1.846 (m, 4H^{CH_2}), 1.453 (m, 4H^{CH_2}), 1.234 (s, 56H^{CH_2}), 0.857 (t, 6H^{CH_3}).

Synthesis of 4,5-Bis(octadecyloxy)benzene-1,2-diamine. The compound 1,2-dinitro-4,5-bis(octadecyloxy)benzene (2.4 g, 3.4 mmol) reacted with 6.3 mL of hydrazine monohydrate and 0.1 g of 10% palladium/carbon in absolute ethanol (50 mL) under inert conditions. The mixture was subsequently allowed to reflux for 18 h and then filtered through Celite under inert conditions. The solvent was reduced to dryness under vacuum to yield a white precipitate. Yield: 76%. ^{1}H NMR ($CDCl_3$, 400 MHz): δ 6.350 (s, 2H^{Ph}) 3.858 (t, 4H^{OCH_2}), 3.121 (s, 4H^{NH_2}), 1.717 (m, 4H^{CH_2}), 1.410 (m, 4H^{CH_2}), 1.234 (s, 56H^{CH_2}), 0.856 (t, 6H^{CH_3}).

Synthesis of *N,N′*-[4,5-Bis(octadecyloxy)-1,2-phenylene]-dipicolineamide ($H_2L^{OC_{18}H_{37}}$). A solution of 4,5-bis(octadecyloxy)-benzene-1,2-diamine (1.05 g, 1.63 mmol) in anhydrous pyridine was cannulated under inert conditions to a mixture of picolinic acid (0.401 g, 3.26 mmol) and triphenyl phosphite (1.01 g, 0.86 mL, 3.26 mmol) in anhydrous pyridine (10 mL). The solution was heated in a water bath for 5 h. Then the product crashed out by the addition of methanol to obtain a pale-yellow precipitate. The precipitate was subsequently filtered and washed with methanol. Yield: 56%. ESI: m/z^+ 855.6721 (100%) for $[C_{54}H_{86}N_4O_4 + H^+]$. IR (KBr, cm^{-1}): 3301 (ν_{N-H}), 2850−2920 (ν_{C-H}), 1660−1680 ($\nu_{C=O}$), 1609, 1591, 1570, 1529 ($\nu_{C=C,aromatic}$ and $\nu_{C=N,pyridine}$), 1236 (ν_{C-O-C}). ^{1}H NMR

DOI: 10.1021/acs.inorgchem.7b03252
Inorg. Chem. 2018, 57, 9748−9756

($CDCl_3$, 400 MHz): δ 10.096 (s, $2H^{NH}$), 8.533 (dd, $2H^{py}$), 8.283 (dd, $2H^{py}$), 7.875 (td, $2H^{py}$), 7.433 (td, $2H^{py}$), 7.407 (s, $2H^{Ph}$), 4.021 (t, $4H^{OCH_2}$), 1.812 (m, $4H^{CH_2}$), 1.488 (m, $4H^{CH_2}$), 1.233 (s, $56H^{CH_2}$), 0.855 (t, $6H^{CH_3}$).

Synthesis of the Complex $[Co^{III}(L^{OC_{18}H_{37}})(pyrr)_2]ClO_4$. The salt of $Co(CH_3COO^-)_2{\cdot}4H_2O$ (0.060 g, 0.240 mmol) dissolved in 1 mL of methanol was added dropwise to 0.200 g (0.232 mmol) of the ligand $L^{OC_{18}H_{37}}$ dissolved in 1 mL of $CHCl_3$. Following this addition, 0.5 mL (excess) of pyrrolidine was added. The solution was stirred overnight at room temperature and then filtered to separate residual solids, and oxygen was bubbled in for 10 min. Precipitation of the microcrystalline product was induced by adding 0.020 g (0.269 mmol) of $NaClO_4$. Multiple attempts to yield crystals for X-ray studies were unfulfilled. Yield: 32 mg, 47%. ESI: m/z^+ 911.58251 (100%) for $[C_{54}H_{84}N_4O_4Co^+]$. IR (KBr, cm^{-1}): 3430 (ν_{N-H}), 2852−2921 (ν_{C-H}), 1625 ($\nu_{C=O}$), 1598 ($\nu_{C=N,pyridine}$), 1207 (ν_{C-O-C}), 1091 (ν_{ClO_4}). ^1H NMR ($CDCl_3$, 600 MHz): δ 9.76 (d, $2H^{py}$), 8.60 (s, $2H^{Ph}$), 8.26 (t, $2H^{py}$), 8.22 (d, $2H^{py}$), 4.06 ($4H^{OCH_2}$), 3.05 ($2H^{NH}$), 2.10 ($4H^{pyr}$), 1.25−1.66 (m, 72H), 0.86 ($6H^{CH_3}$). Anal. Calcd for $[C_{62}H_{102}CoN_6O_8Cl]$: C, 64.54; H, 8.91; N, 7.28. Found: C, 64.49; H, 8.91; N, 7.02.

Ink Preparation. CB (6 mg) was suspended in CH_2Cl_2 and sonicated for 5 min. Following sonication, 0.125 mL of a stock solution of $[Co^{III}(L^{OC_{18}H_{37}})(pyrr)_2]ClO_4$ (4 mg/mL in CH_2Cl_2) was added to CB. The mixture was sonicated for a further 15 min. Following sonication, ∼40 mL of ethanol was added to the CB suspension. The suspension was centrifuged, the solvent was decanted, and CB was allowed to dry overnight under ambient conditions. The dry carbon sample was suspended in 0.300 mL of water, 0.600 mL of ethanol, and 0.300 mL of isopropyl alcohol. This suspension was sonicated for 15 min, and then 0.300 mL of Nafion was added. The suspension was further sonicated for 15 min to form the ink used for catalysis. On the basis of the initial amount of **1** added, we expect the final concentration of cobalt in the ink to be 15.6 μg/mL; however, ICP-MS analysis revealed that the actual concentration of cobalt in the ink is 10.9 μg/mL, which is a 70% adsorption efficiency.

Catalytic Measurements. *Cyclic Voltammetry.* All cyclic voltammograms were recorded using an EC Epsilon potentiostat equipped with an RDE2 rotating-disk electrode. The three-electrode setup included an Ag/AgCl reference electrode, a platinum wire auxiliary electrode, and a glassy carbon working electrode (surface area = 0.07 cm^2). A total of 5 μL of the ink was deposited on the glassy carbon surface of the working electrode and dried under an IR heat lamp for 5 min. The cyclic voltammograms were measured at a scan rate of 10 mV/s at 1600 rpm in a 1 M KOH solution. After the potentials against Ag/AgCl were measured, they were converted to the standard hydrogen electrode (RHE) using eq 1. Additionally, using the *iR* compensation function of the *Epsilon* software, the resistivity of the solution was measured, and corrections were calculated using eq 2.

$$E_{SHE} = E_{Ag/AgCl} + 0.197 \tag{1}$$

$$E_{SHE} = E_{Ag/AgCl} + 0.197 - iR \tag{2}$$

Bulk Electrolysis and Faradaic Efficiency. Bulk electrolysis was performed under an overpotential of 0.49 V in a custom H-type cell that is split into two compartments by a fine frit. The auxiliary electrode, a platinum coil, was placed in one compartment, and the reference (Ag/AgCl) and working electrodes were placed in the other. The working electrode was prepared by depositing 100 μL of the functionalized ink (contains 0.02 μmol of **1**) onto a 1 cm × 4 cm piece of carbon cloth, allowing it to dry for 15 min, and threading it onto a copper wire. A GOW-MAC series 400 gas chromatograph equipped with a thermal conductivity detector and a 8 ft × $^1/_8$ in., 5 Å molecular sieve column held at 60 °C were used to quantify the amount of oxygen produced. Helium was used as the carrier gas and flowed at a rate of 30 mL/min. Atmospheric nitrogen was used as an internal standard.

Computational Methods. Electronic structure calculations were performed using the *Gaussian* series of programs (*Gaussian09*, revision E01).[47] DFT calculations were carried out using the B3LYP* functional.[48] Geometries were optimized using B3LYP* with the SDD basis set with an effective core potential[49] for the cobalt atom and the 6-31G(d,p) basis set for all other atoms. The energetics of structures with different spin states were compared, and the lowest energy structures were used for the proposed catalytic cycle. The structures with the lowest Gibbs free energy were reoptimized with the SDD (for the cobalt atom) and 6-31+G(d,p) (for all other atoms) basis sets to obtain more accurate energies.[50,51] The SMD implicit solvation model was used to incorporate solvation effects in water and included in all of the geometry optimizations.[52] Previous studies[53−56] have shown that a small number of explicit water molecules need to be included to account for some of the short-range interactions while modeling anions such as OH^- in aqueous solution using the SMD implicit solvation model. Therefore, the lowest-energy structures involved in the catalytic cycle were optimized, with two explicit water molecules forming hydrogen bonds with $OH/O^-/OOH/OO^-$ moieties in SMD implicit solvation. All of the geometries were confirmed to be minima on the potential energy surfaces by performing a vibrational frequency calculation and had no imaginary frequency. Thermal and entropy contributions to the free energies were calculated by standard statistical thermodynamical methods using unscaled B3LYP* frequencies and a rigid rotor/harmonic oscillator approximation at 298.15 K. The converged wave functions were tested for self-consistent-field stability.

For a redox reaction, $A(aq) \rightarrow A^{n+}(aq) + ne-(aq)$, the standard redox potential is given by eq 3, where $\Delta G_{aq}^* = G_{A(aq)}^* - G_{A^{n+}(aq)}^* - G_{e(g)}^*$ is the standard free energy change for a redox couple in solution, $G_{e(g)}^* = 0.867$ kcal/mol is the free energy of the electron at 298.15 K,[53,57] obtained from the literature, F is Faraday's constant (23.06 kcal/mol·V), n is the number of electrons, and SHE is the absolute potential of the standard hydrogen electrode (4.281 V).[58−60]

$$E_{aq}^\circ = \frac{-\Delta G_{aq}^*}{nF} - \text{SHE} \tag{3}$$

The pH-dependent redox potential can be obtained by solving the Nernst half-cell equation where E° is the standard redox potential (eq 4). The redox potential at a particular pH can be obtained by including the equilibrium concentration of each of the relevant species at that pH using acid dissociation constants (K_a's). For low ionic strength, the pH-dependent redox potential is given by eq 5, where AH is the reduced form, $AH^{\bullet+}$ is the one-electron-oxidized form, and A● is the oxidized form after the proton-coupled electron-transfer process.

$$E_{1/2} = E^\circ - \frac{RT}{nF}\ln\left(\frac{[\text{Red}]}{[\text{Ox}]}\right) \tag{4}$$

$$E_{pH} = E_{A^\bullet,H^+/AH}^\circ - \frac{RT}{nF}\ln\left(\frac{10^{-pK_a} + 10^{-pH}}{10^{-(pK_a+pH)}}\right) \tag{5}$$

The aqueous-phase free energy of the proton is calculated as in eq 6, where $\Delta G_{H^+(aq)}^* = -265.9$ kcal/mol is the solvation energy of the proton taken from the literature,[58−60] $G_{H^+(g)}^\circ = -6.29$ kcal/mol is the gas-phase standard free energy of the proton, and $\Delta G^{corr} = 1.89$ kcal/mol is the correction term for conversion of a standard state of 1 atm in the gas phase to the standard state of a 1 M solution.[57,61]

$$G_{H^+(aq)}^* = G_{H^+(g)}^\circ - \Delta G_{H^+(aq)}^* - \Delta G^{corr} \tag{6}$$

EPR Spectroscopy. Continuous-wave (cw) X-band (9−10 GHz) EPR experiments were carried out with a Bruker ELEXSYS II E500 EPR spectrometer (Bruker Biospin, Rheinstetten, Germany), equipped with a TE_{102} rectangular EPR resonator (Bruker ER 4102ST) and a helium gas-flow cryostat (ICE Oxford, U.K.). An intelligent temperature controller (ITC503) from Oxford Instruments, Oxford, U.K., was used. Measurements on the frozen solutions were done at a cryogenic temperature (T = 30 K). Data processing was done using *Xepr* (Bruker BioSpin, Rheinstetten, Germany) and *Matlab 7.11.2* (The MathWorks, Inc., Natick, MA) environments.

DOI: 10.1021/acs.inorgchem.7b03252
Inorg. Chem. 2018, 57, 9748−9756

■ ASSOCIATED CONTENT

Supporting Information

The Supporting Information is available free of charge on the ACS Publications website at DOI: 10.1021/acs.inorgchem.7b03252.

Experimental procedures and select figures (PDF)

■ AUTHOR INFORMATION

Corresponding Author

*E-mail: cnverani@chem.wayne.edu.

ORCID

Jens Niklas: 0000-0002-6462-2680
Oleg G. Poluektov: 0000-0003-3067-9272
H. Bernhard Schlegel: 0000-0001-7114-2821
Cláudio N. Verani: 0000-0001-6482-1738

Notes

The authors declare no competing financial interest.

■ ACKNOWLEDGMENTS

The authors thankfully acknowledge support from the National Science Foundation (Grant NSF-CHE-1500201 to C.N.V. and Grant NSF-CHE1464450 to H.B.S.) and from the U.S. Department of Energy, Office of Science, Office of Basic Energy Sciences (Grant DE-SC0001907 to C.N.V. and H.B.S. and Contract DE-AC02-06CH11357 to J.N. and O.G.P. at ANL). Jordyn Burdick is an undergraduate researcher.

■ REFERENCES

(1) Garrido-Barros, P.; Funes-Ardoiz, I.; Drouet, S.; Benet-Buchholz, J.; Maseras, F.; Llobet, A. Redox Non-innocent Ligand Controls Water Oxidation Overpotential in a New Family of Mononuclear Cu-Based Efficient Catalysts. *J. Am. Chem. Soc.* **2015**, *137*, 6758−6761.

(2) Nakazono, T.; Parent, A. R.; Sakai, K. Improving Singlet Oxygen Resistance during Photochemical Water Oxidation by Cobalt Porphyrin Catalysts. *Chem. - Eur. J.* **2015**, *21*, 6723−6726.

(3) Lyaskovskyy, V.; de Bruin, B. Redox Non-Innocent Ligands: Versatile New Tools to Control Catalytic Reactions. *ACS Catal.* **2012**, *2*, 270−279.

(4) Lei, H.; Liu, C.; Wang, Z.; Zhang, Z.; Zhang, M.; Chang, X.; Zhang, W.; Cao, R. Noncovalent Immobilization of a Pyrene-Modified Cobalt Corrole on Carbon Supports for Enhanced Electrocatalytic Oxygen Reduction and Oxygen Evolution in Aqueous Solutions. *ACS Catal.* **2016**, *6*, 6429−6437.

(5) Li, F.; Zhang, B.; Li, X.; Jiang, Y.; Chen, L.; Li, Y.; Sun, L. Highly Efficient Oxidation of Water by a Molecular Catalyst Immobilized on Carbon Nanotubes. *Angew. Chem., Int. Ed.* **2011**, *50*, 12276−12279.

(6) Li, F.; Li, L.; Tong, L.; Daniel, Q.; Gothelid, M.; Sun, L. Immobilization of a molecular catalyst on carbon nanotubes for highly efficient electro-catalytic water oxidation. *Chem. Commun.* **2014**, *50*, 13948−13951.

(7) Gonawala, S.; Baydoun, H.; Wickramasinghe, L.; Verani, C. N. Efficient water oxidation with electromodified Langmuir-Blodgett films of procatalytic [$Co^{III}(N_2O_3)$] metallosurfactants on electrodes. *Chem. Commun.* **2016**, *52*, 8440−8443.

(8) Li, D.; Baydoun, H.; Verani, C. N.; Brock, S. L. Efficient Water Oxidation Using CoMnP Nanoparticles. *J. Am. Chem. Soc.* **2016**, *138*, 4006−4009.

(9) Li, D.; Baydoun, H.; Kulikowski, B.; Brock, S. L. Boosting the Catalytic Performance of Iron Phosphide Nanorods for the Oxygen Evolution Reaction by Incorporation of Manganese. *Chem. Mater.* **2017**, *29*, 3048−3054.

(10) Liyanage, D. R.; Li, D.; Cheek, Q. B.; Baydoun, H.; Brock, S. L. Synthesis and oxygen evolution reaction (OER) catalytic performance of Ni_2-xRuxP nanocrystals: enhancing activity by dilution of the noble metal. *J. Mater. Chem. A* **2017**, *5*, 17609−17618.

(11) Wickramasinghe, L. D.; Perera, M. M.; Li, L.; Mao, G. Z.; Zhou, Z. X.; Verani, C. N. Rectification in Nanoscale Devices Based on an Asymmetric Five-Coordinate Iron(III) Phenolate Complex. *Angew. Chem., Int. Ed.* **2013**, *52*, 13346−13350.

(12) Wickramasinghe, L. D.; Mazumder, S.; Gonawala, S.; Perera, M. M.; Baydoun, H.; Thapa, B.; Li, L.; Xie, L.; Mao, G.; Zhou, Z.; Schlegel, H. B.; Verani, C. N. The Mechanisms of Rectification in Au|MoleculelAu Devices Based on Langmuir−Blodgett Monolayers of Iron(III) and Copper(II) Surfactants. *Angew. Chem., Int. Ed.* **2014**, *53*, 14462−14467.

(13) Gonawala, S.; Leopoldino, V. R.; Kpogo, K.; Verani, C. N. Langmuir-Blodgett films of salophen-based metallosurfactants as surface pretreatment coatings for corrosion mitigation. *Chem. Commun.* **2016**, *52*, 11155−11158.

(14) Wickramasinghe, L. *Redox-Active Trivalent Metallosurfactants with Low Global Symmetry for Molecule-Based Electronics: Spectroscopic, Electrochemical, and Amphiphilic Properties of New Molecular Materials for Current−Voltage Measurements in M|lb-Monolayer|m Devices*; Wayne State University: Detroit, MI, 2014.

(15) Johnson, M. S.; Wickramasinghe, L.; Verani, C.; Metzger, R. M. Confirmation of the Rectifying Behavior in a Pentacoordinate [N2O2] Iron(III) Surfactant Using a "Eutectic GaIn | LB Monolayer | Au" Assembly. *J. Phys. Chem. C* **2016**, *120*, 10578−10583.

(16) Barnes, D. J.; Chapman, R. L.; Vagg, R. S.; Watton, E. C. Synthesis of novel bis(amides) by means of triphenyl phosphite intermediates. *J. Chem. Eng. Data* **1978**, *23*, 349−350.

(17) Amirnasr, M.; Schenk, K. J.; Meghdadi, S. Synthesis and characterization of trans-[Co(III)(bpb)(amine)2]X (X = NCS, ClO_4). X-ray crystal structure of trans-[Co(III)(bpb)(pyrrolidine)$_2$]NCS·0.5H_2O containing intermolecular N-H···O═C hydrogen-bonding. *Inorg. Chim. Acta* **2002**, *338*, 19−26.

(18) Meghdadi, S.; Amirnasr, M.; Habibi, M. H.; Amiri, A.; Ghodsi, V.; Rohani, A.; Harrington, R. W.; Clegg, W. Synthesis, structure, and electrochemistry of pyridinecarboxamide cobalt(III) complexes; the effect of bridge substituents on the redox properties. *Polyhedron* **2008**, *27*, 2771−2778.

(19) Gagne, R. R.; Koval, C. A.; Lisensky, G. C. Ferrocene as an internal standard for electrochemical measurements. *Inorg. Chem.* **1980**, *19*, 2854−2855.

(20) Dutta, S. K.; Beckmann, U.; Bill, E.; Weyhermüller, T.; Wieghardt, K. 1,2-Bis(pyridine-2-carboxamido)benzenate(2−), (bpb)-2-: A Noninnocent Ligand. Syntheses, Structures, and Mechanisms of Formation of [(n-Bu)$_4$N][Fe^{IV}_2(μ-N)(bpb)$_2$(X)$_2$] (X = CN^-, N^{3-}) and the Electronic Structures of [M^{III}(bpbox1)(CN)$_2$] (M = Co, Fe). *Inorg. Chem.* **2000**, *39*, 3355−3364.

(21) Beckmann, U.; Bill, E.; Weyhermüller, T.; Wieghardt, K. Dinuclear Cyano Complexes of Cobalt(III) and Iron(III) Containing Noninnocent 1,2,4,5-Tetrakis(2-pyridinecarboxamido)benzene Bridging Ligands. *Inorg. Chem.* **2003**, *42*, 1045−1056.

(22) Baydoun, H.; Mazumder, S.; Schlegel, H. B.; Verani, C. N. Deactivation of a Cobalt Catalyst for Water Reduction through Valence Tautomerism. *Chem. - Eur. J.* **2017**, *23*, 9266−9271.

(23) Hu, B.; Getsoian, A. B.; Schweitzer, N. M.; Das, U.; Kim, H.; Niklas, J.; Poluektov, O.; Curtiss, L. A.; Stair, P. C.; Miller, J. T.; Hock, A. S. Selective propane dehydrogenation with single-site CoII on SiO2 by a non-redox mechanism. *J. Catal.* **2015**, *322*, 24−37.

(24) Niklas, J.; Mardis, K. L.; Rakhimov, R. R.; Mulfort, K. L.; Tiede, D. M.; Poluektov, O. G. The Hydrogen Catalyst Cobaloxime: A Multifrequency EPR and DFT Study of Cobaloxime's Electronic Structure. *J. Phys. Chem. B* **2012**, *116*, 2943−2957.

(25) Basu, D.; Mazumder, S.; Niklas, J.; Baydoun, H.; Wanniarachchi, D.; Shi, X.; Staples, R. J.; Poluektov, O.; Schlegel, H. B.; Verani, C. N. Evaluation of the coordination preferences and catalytic pathways of heteroaxial cobalt oximes towards hydrogen generation. *Chem. Sci.* **2016**, *7*, 3264−3278.

(26) Wickramasinghe, L. D.; Mazumder, S.; Gonawala, S.; Perera, M. M.; Baydoun, H.; Thapa, B.; Li, L.; Xie, L. X.; Mao, G. Z.; Zhou, Z. X.;

DOI: 10.1021/acs.inorgchem.7b03252
Inorg. Chem. 2018, 57, 9748−9756

Schlegel, H. B.; Verani, C. N. The Mechanisms of Rectification in Au | Molecule | Au Devices Based on Langmuir-Blodgett Monolayers of Iron(III) and Copper(II) Surfactants. *Angew. Chem., Int. Ed.* **2014**, *53*, 14462−14467.
(27) Kärkäs, M. D.; Åkermark, T.; Chen, H.; Sun, J.; Åkermark, B. A Tailor-Made Molecular Ruthenium Catalyst for the Oxidation of Water and Its Deactivation through Poisoning by Carbon Monoxide. *Angew. Chem., Int. Ed.* **2013**, *52*, 4189−4193.
(28) Lee, S. H.; Han, J. H.; Kwak, H.; Lee, S. J.; Lee, E. Y.; Kim, H. J.; Lee, J. H.; Bae, C.; Lee, S. N.; Kim, Y.; Kim, C. Biomimetic Hydrocarbon Oxidation Catalyzed by Nonheme Iron(III) Complexes with Peracids: Evidence for an FeV = O Species. *Chem. - Eur. J.* **2007**, *13*, 9393−9398.
(29) Song, Y. J.; Hyun, M. Y.; Lee, J. H.; Lee, H. G.; Kim, J. H.; Jang, S. P.; Noh, J. Y.; Kim, Y.; Kim, S.-J.; Lee, S. J.; Kim, C. Amide-Based Nonheme Cobalt(III) Olefin Epoxidation Catalyst: Partition of Multiple Active Oxidants CoV = O, CoIV = O, and CoIII-OO(O)CR. *Chem. - Eur. J.* **2012**, *18*, 6094−6101.
(30) Song, Y. J.; Lee, S. H.; Park, H. M.; Kim, S. H.; Goo, H. G.; Eom, G. H.; Lee, J. H.; Lah, M. S.; Kim, Y.; Kim, S.-J.; Lee, J. E.; Lee, H.-I.; Kim, C. Robust and Efficient Amide-Based Nonheme Manganese(III) Hydrocarbon Oxidation Catalysts: Substrate and Solvent Effects on Involvement and Partition of Multiple Active Oxidants. *Chem. - Eur. J.* **2011**, *17*, 7336−7344.
(31) McCrory, C. C. L.; Jung, S.; Peters, J. C.; Jaramillo, T. F. Benchmarking Heterogeneous Electrocatalysts for the Oxygen Evolution Reaction. *J. Am. Chem. Soc.* **2013**, *135*, 16977−16987.
(32) Galán-Mascarós, J. R. Water Oxidation at Electrodes Modified with Earth-Abundant Transition-Metal Catalysts. *ChemElectroChem* **2015**, *2*, 37−50.
(33) Tahir, M.; Pan, L.; Idrees, F.; Zhang, X.; Wang, L.; Zou, J.-J.; Wang, Z. L. Electrocatalytic oxygen evolution reaction for energy conversion and storage: A comprehensive review. *Nano Energy* **2017**, *37*, 136−157.
(34) Suen, N.-T.; Hung, S.-F.; Quan, Q.; Zhang, N.; Xu, Y.-J.; Chen, H. M. Electrocatalysis for the oxygen evolution reaction: recent development and future perspectives. *Chem. Soc. Rev.* **2017**, *46*, 337−365.
(35) Lee, W.-T.; Muñoz, S. B.; Dickie, D. A.; Smith, J. M. Ligand Modification Transforms a Catalase Mimic into a Water Oxidation Catalyst. *Angew. Chem., Int. Ed.* **2014**, *53*, 9856−9859.
(36) Nakazono, T.; Parent, A. R.; Sakai, K. Cobalt porphyrins as homogeneous catalysts for water oxidation. *Chem. Commun.* **2013**, *49*, 6325−6327.
(37) Ishizuka, T.; Watanabe, A.; Kotani, H.; Hong, D.; Satonaka, K.; Wada, T.; Shiota, Y.; Yoshizawa, K.; Ohara, K.; Yamaguchi, K.; Kato, S.; Fukuzumi, S.; Kojima, T. Homogeneous Photocatalytic Water Oxidation with a Dinuclear CoIII−Pyridylmethylamine Complex. *Inorg. Chem.* **2016**, *55*, 1154−1164.
(38) Parent, A. R.; Sakai, K. Progress in Base-Metal Water Oxidation Catalysis. *ChemSusChem* **2014**, *7*, 2070−2080.
(39) Downes, C. A.; Marinescu, S. C. Efficient Electrochemical and Photoelectrochemical H_2 Production from Water by a Cobalt Dithiolene One-Dimensional Metal−Organic Surface. *J. Am. Chem. Soc.* **2015**, *137*, 13740−13743.
(40) Marenich, A. V.; Ho, J.; Coote, M. L.; Cramer, C. J.; Truhlar, D. G. Computational electrochemistry: prediction of liquid-phase reduction potentials. *Phys. Chem. Chem. Phys.* **2014**, *16*, 15068−15106.
(41) Panda, C.; Debgupta, J.; Díaz Díaz, D.; Singh, K. K.; Sen Gupta, S.; Dhar, B. B. Homogeneous Photochemical Water Oxidation by Biuret-Modified Fe-TAML: Evidence of FeV(O) Intermediate. *J. Am. Chem. Soc.* **2014**, *136*, 12273−12282.
(42) Das, D.; Pattanayak, S.; Singh, K. K.; Garai, B.; Sen Gupta, S. Electrocatalytic water oxidation by a molecular cobalt complex through a high valent cobalt oxo intermediate. *Chem. Commun.* **2016**, *52*, 11787−11790.
(43) Wang, C.-C.; Chang, H.-C.; Lai, Y.-C.; Fang, H.; Li, C.-C.; Hsu, H.-K.; Li, Z.-Y.; Lin, T.-S.; Kuo, T.-S.; Neese, F.; Ye, S.; Chiang, Y.-W.; Tsai, M.-L.; Liaw, W.-F.; Lee, W.-Z. A Structurally Characterized Nonheme Cobalt−Hydroperoxo Complex Derived from Its Superoxo Intermediate via Hydrogen Atom Abstraction. *J. Am. Chem. Soc.* **2016**, *138*, 14186−14189.
(44) Wang, B.; Lee, Y.-M.; Tcho, W.-Y.; Tussupbayev, S.; Kim, S.-T.; Kim, Y.; Seo, M. S.; Cho, K.-B.; Dede, Y.; Keegan, B. C.; Ogura, T.; Kim, S. H.; Ohta, T.; Baik, M.-H.; Ray, K.; Shearer, J.; Nam, W. *Nat. Commun.* **2017**, *8*, 14839.
(45) Pfaff, F. F.; Kundu, S.; Risch, M.; Pandian, S.; Heims, F.; Pryjomska-Ray, I.; Haack, P.; Metzinger, R.; Bill, E.; Dau, H.; Comba, P.; Ray, K. An Oxocobalt(IV) Complex Stabilized by Lewis Acid Interactions with Scandium(III) Ions. *Angew. Chem., Int. Ed.* **2011**, *50*, 1711−1715.
(46) Liao, R.-Z.; Li, X.-C.; Siegbahn, P. E. M. Reaction Mechanism of Water Oxidation Catalyzed by Iron Tetraamido Macrocyclic Ligand Complexes − A DFT Study. *Eur. J. Inorg. Chem.* **2014**, *2014*, 728−741.
(47) Frisch, M. J.; Trucks, G. W.; Schlegel, H. B.; Scuseria, G. E.; Robb, M. A.; Cheeseman, J. R.; Scalmani, G.; Barone, V.; Petersson, G. A.; Nakatsuji, H.; Li, X.; Caricato, M.; Marenich, A.; Bloino, J.; Janesko, B. G.; Gomperts, R.; Mennucci, B.; Hratchian, H. P.; Ortiz, J. V.; Izmaylov, A. F.; Sonnenberg, J. L.; Williams-Young, D.; Ding, F.; Lipparini, F.; Egidi, F.; Goings, J.; Peng, B.; Petrone, A.; Henderson, T.; Ranasinghe, D.; Zakrzewski, V. G.; Gao, J.; Rega, N.; Zheng, G.; Liang, W.; Hada, M.; Ehara, M.; Toyota, K.; Fukuda, R.; Hasegawa, J.; Ishida, M.; Nakajima, T.; Honda, Y.; Kitao, O.; Nakai, H.; Vreven, T.; Throssell, K.; Montgomery, J. A., Jr.; Peralta, J. E.; Ogliaro, F.; Bearpark, M.; Heyd, J. J.; Brothers, E.; Kudin, K. N.; Staroverov, V. N.; Keith, T.; Kobayashi, R.; Normand, J.; Raghavachari, K.; Rendell, A.; Burant, J. C.; Iyengar, S. S.; Tomasi, J.; Cossi, M.; Millam, J. M.; Klene, M.; Adamo, C.; Cammi, R.; Ochterski, J. W.; Martin, R. L.; Morokuma, K.; Farkas, O.; Foresman, J. B.; Fox, D. J. *Gaussian09*, revision E01; Gaussian, Inc.: Wallingford, CT, 2016.
(48) Reiher, M.; Salomon, O.; Artur Hess, B. Reparameterization of hybrid functionals based on energy differences of states of different multiplicity. *Theor. Chem. Acc.* **2001**, *107*, 48−55.
(49) Dolg, M.; Wedig, U.; Stoll, H.; Preuss, H. Energy-adjusted ab initio pseudopotentials for the first row transition elements. *J. Chem. Phys.* **1987**, *86*, 866−872.
(50) Francl, M. M.; Pietro, W. J.; Hehre, W. J.; Binkley, J. S.; Gordon, M. S.; DeFrees, D. J.; Pople, J. A. Self-consistent molecular orbital methods. XXIII. A polarization-type basis set for second-row elements. *J. Chem. Phys.* **1982**, *77*, 3654−3665.
(51) Hariharan, P. C.; Pople, J. A. The influence of polarization functions on molecular orbital hydrogenation energies. *Theor. Chim. Acta* **1973**, *28*, 213−222.
(52) Marenich, A. V.; Cramer, C. J.; Truhlar, D. G. Universal Solvation Model Based on Solute Electron Density and on a Continuum Model of the Solvent Defined by the Bulk Dielectric Constant and Atomic Surface Tensions. *J. Phys. Chem. B* **2009**, *113*, 6378−6396.
(53) Thapa, B.; Schlegel, H. B. Calculations of pKa's and Redox Potentials of Nucleobases with Explicit Waters and Polarizable Continuum Solvation. *J. Phys. Chem. A* **2015**, *119*, 5134−5144.
(54) Thapa, B.; Schlegel, H. B. Theoretical Calculation of pKa's of Selenols in Aqueous Solution Using an Implicit Solvation Model and Explicit Water Molecules. *J. Phys. Chem. A* **2016**, *120*, 8916−8922.
(55) Thapa, B.; Schlegel, H. B. Density Functional Theory Calculation of pKa's of Thiols in Aqueous Solution Using Explicit Water Molecules and the Polarizable Continuum Model. *J. Phys. Chem. A* **2016**, *120*, 5726−5735.
(56) Thapa, B.; Schlegel, H. B. Improved pKa Prediction of Substituted Alcohols, Phenols, and Hydroperoxides in Aqueous Medium Using Density Functional Theory and a Cluster-Continuum Solvation Model. *J. Phys. Chem. A* **2017**, *121*, 4698−4706.
(57) Bartmess, J. E. Thermodynamics of the electron and the proton. *J. Phys. Chem.* **1994**, *98*, 6420−6424.
(58) Camaioni, D. M.; Schwerdtfeger, C. A. Comment on "Accurate experimental values for the free energies of hydration of H+, OH-, and H3O+. *J. Phys. Chem. A* **2005**, *109*, 10795−10797.

DOI: 10.1021/acs.inorgchem.7b03252
Inorg. Chem. 2018, 57, 9748−9756

(59) Isse, A. A.; Gennaro, A. Absolute potential of the standard hydrogen electrode and the problem of interconversion of potentials in different solvents. *J. Phys. Chem. B* **2010**, *114*, 7894−7899.
(60) Kelly, C. P.; Cramer, C. J.; Truhlar, D. G. Aqueous solvation free energies of ions and ion− water clusters based on an accurate value for the absolute aqueous solvation free energy of the proton. *J. Phys. Chem. B* **2006**, *110*, 16066−16081.
(61) Ben-Naim, A.; Marcus, Y. Solvation thermodynamics of nonionic solutes. *J. Chem. Phys.* **1984**, *81*, 2016−2027.

DOI: 10.1021/acs.inorgchem.7b03252
Inorg. Chem. 2018, 57, 9748−9756